Dynamics of feature binding during object-selective attention

M. A. Schoenfeld*, C. Tempelmann*, A. Martinez[†‡], J.-M. Hopf*, C. Sattler[§], H.-J. Heinze*, and S. A. Hillyard[†¶]

*Department of Neurology II, Otto von Guericke University, 31920 Magdeburg, Germany; [†]Department of Neurosciences, University of California at San Diego, La Jolla, CA 92093; [‡]Nathan Kline Institute for Psychiatric Research, Orangeburg, NY 10962; and [§]Department of Psychology, Friedrich Schiller University, 07743 Jena, Germany

Edited by Michael I. Posner, University of Oregon, Eugene, OR, and approved July 29, 2003 (received for review May 9, 2003)

Objects in the environment may be attended selectively and perceived as unified ensembles of their constituent features. To investigate the timing and cortical localization of feature-integration mechanisms in object-based attention, recordings of event-related potentials and magnetic fields were combined with functional MRI while subjects attended to one of two superimposed transparent surfaces formed by arrays of dots moving in opposite directions. A spatiotemporal analysis revealed evidence for a rapid increase in neural activity localized to a color-selective region of the fusiform gyrus when the surface moving in the attended direction displayed an irrelevant color feature. These data provide support for the ''integrated-competition'' model of object-selective attention and point to a dynamic neural substrate for the rapid binding process that links relevant and irrelevant features to form a unified perceptual object.

Everyday visual scenes often include a multitude of objects that differ in their contours, feature constituents, and locations in the visual field. Specific objects may be selected for preferential processing and action by directing attention to their locations (1) or to their individual features such as color or shape (2–4). There is mounting evidence that visual attention may also select out whole objects as integrated feature ensembles (5–13). Little is known, however, about the neural mechanisms that enable the different features of objects, which may be represented in widely dispersed cortical areas, to be bound together into a unified percept (14).

Neurophysiological studies in monkeys have led to theoretical proposals that attempt to account for object-based attentional selection. According to the ''biased-competition'' hypothesis (15–17), the neural representations of neighboring objects are mutually inhibitory and compete with one another for precedence. This competition may be biased by both bottom-up factors such as stimulus intensity and by top-down factors such as task relevance and attention. Duncan (18) has proposed further that this competition between objects is integrated across the different cortical regions that encode their constituent features. Thus, when attention is directed to one feature of an object, all of its features will tend to become dominant in their respective cortical modules, and the selected object will gain competitive advantage throughout the network of interconnected feature-specific areas.

A key prediction of this ''integrated-competition'' model (18, 19) is that directing attention to one feature of an object will result in the selection of its other features, not only those relevant to the task at hand but also currently irrelevant features. Physiological evidence for such selection comes from a neuroimaging study by O'Craven *et al.* (20) in which subjects were directed to attend to pictures of either houses or faces that were superimposed to preclude selection by spatial attention. On a given run, either the house or the face image was continually in motion. It was found by using functional MRI (fMRI) that neural activity was increased not only in the cortical area specific to the attended stimulus attribute (for faces, the fusiform face area; for houses, the hippocampal place area; for motion, the middle temporal area) but also in the area encoding the task-irrelevant attribute of the attended object.

The study by O'Craven *et al.* (20) provides evidence for an object-based attention mechanism that selects irrelevant features of an attended object in their respective cortical modules. Because of the limited time resolution of fMRI, however, the dynamic properties and functional significance of this mechanism remain unclear. In particular, with fMRI it is not possible to determine whether such a selection of irrelevant features occurs rapidly enough to participate in the feature-integration processes that lead to the perception of a unified attended object. The present study investigated this question by recording event-related potentials (ERPs) and event-related magnetic fields (ERFs) together with fMRI while subjects attended to multifeature objects formed by moving-dot arrays. This spatiotemporal analysis found that an irrelevant feature (color) was activated in its specialized cortical module within a few tens of milliseconds after initial registration, rapidly enough to provide a mechanism for the binding and perceptual integration of the multiple features of an attended object.

Methods

Subjects. Eight healthy subjects (four male, ages 21–27 years) with normal color vision and normal or corrected-to-normal acuity participated as paid volunteers in the ERP/ERF experiment. Four of these subjects (three male) also participated in the fMRI experiment. All gave informed consent, and the study was approved by the local ethics committee.

Stimuli. In the ERP/ERF experiment, moving-dot stimuli were presented on a video monitor situated 120 cm in front of the subject. Stimuli were presented against a dark background (0.22 cd/m^2) within a square region ($4° \times 4°$) that was centered on the vertical meridian 3° above a central fixation cross (to the lower edge of the square). One hundred stationary white dots (200 cd/m^2) were present continuously in this square during the intertrial intervals. At the start of each trial a random half of the dots moved coherently to the left while the other half moved simultaneously to the right for 300 ms. Each dot population was colored uniformly, and they were perceived as two transparent surfaces moving in opposite directions. The task-irrelevant color could either be maintained as white (the same as in the intertrial interval) or changed to an isoluminant red during the 300-ms period of movement. Red/white isoluminance was established through heterochromatic flicker photometry.

The color of the left- or right-moving dots could be either red or white on a pseudorandom basis, leading to three basic

This paper was submitted directly (Track II) to the PNAS office.

Abbreviations: fMRI, functional MRI; ERP, event-related potential; ERF, event-related magnetic field; RT, reaction time; ns, not significant.

[¶]To whom correspondence should be addressed at: Department of Neurosciences 0608, University of California at San Diego, 9500 Gilman Drive, La Jolla, CA 92093-0608. E-mail: shillyard@ucsd.edu.

 www.pnas.org/cgi/doi/10.1073/pnas.1932820100

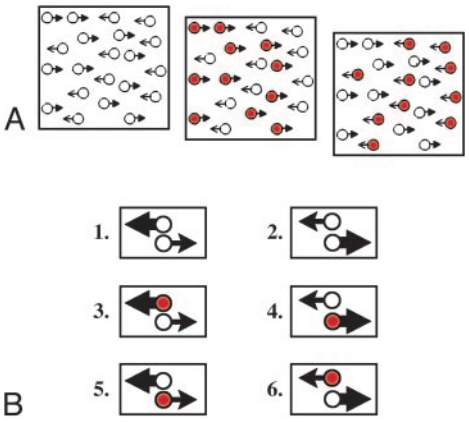

Fig. 1. (*A*) Schematic diagram of the three possible stimulus configurations, which were presented equiprobably in random order. The right-moving or left-moving dot arrays could be either red or white. Bold arrows indicate the attended direction, which in this example is rightward. On some trials, the dots moving in one or both directions had a higher velocity, and subjects responded to those in the attended direction as targets. (*B*) The six experimental conditions defined by the colors of the left- and right-moving dots and direction of attention.

stimulus combinations (see Fig. 1): red-left/white-right, white-left/red-right, and white-left/white-right. Also on a pseudorandom basis, the velocity of the dot movement in either direction could be either slow (4°/s, on 75% of the trials) or fast (7°/s, on 25% of the trials). The intertrial interval varied randomly between 1.2 and 2.0 s, after which the 100 stationary dots were randomly reassigned to either the right- or left-moving surfaces.

During the fMRI experiment the stimuli were presented via a projector/mirror system. The stimulus parameters were identical to those of the ERP/ERF sessions, except that the intertrial interval was varied between 1.0 and 7.0 s following a gamma function to allow trial separation in an event-related analysis.

Procedure. Before each block of 16 trials, a symbolic cue (arrow pointing to the left or right) replaced the fixation cross for 2 s, indicating to the subjects which direction of movement (i.e., which surface) was to be attended on that block. On each block a target stimulus (fast movement in the attended direction) could occur one to three times at random. Subjects were instructed to press a button as quickly as possible after detecting a target and to ignore the colors of the dots. After 16 trials a new cue appeared, which was followed by the next block of trials. Each experimental run consisted of 10 blocks and had a duration of either 5–6 min (ERP/ERF recordings) or 8–9 min (fMRI). Before the experimental sessions, subjects were trained to maintain fixation on the central cross during task performance as verified by recording the electrooculogram.

ERP/ERF Recordings. ***Data acquisition.*** ERPs and ERFs were recorded simultaneously by using a BTI Magnes 2500 WH (Biomagnetic Technology, San Diego) whole-head system with 148 magnetometer channels and 32 electroencephalogram channels (NeuroScan, El Paso, TX). Recording bandpass was DC-50 Hz bandpass with a sampling rate of 254 Hz. Artifact rejection was performed offline by removing epochs with peak-to-peak amplitudes exceeding a threshold of 3.0×10^{-12} T, as well as epochs before, during, and after button presses. Individual head shapes were coregistered with the sensor coordinate system by digitizing (Polhemus 3-Space Fastrak, Colchester, VT) skull landmarks (nasion, left and right preauricular points) and determining their locations relative to sensor and electrode positions by using signals from five distributed head coils. These landmarks enabled coregistration of ERP/ERF activity with individual anatomical magnetic resonance scans that were used to help constrain realistic source reconstruction. Fixation was monitored with vertical and horizontal electrooculogram recordings.

Table 1. Talairach coordinates of fMRI activations and dipolar sources

Condition	*x*	*y*	*z*
fMRI sensory	−24.9	−68.1	−5.0
	22.6	−66.9	−6.2
ERP/ERF sensory	−22.8	−66.3	−5.0
	22.9	−65.8	−5.0
fMRI attention	−25.4	−68.3	−4.3
	23.1	−67.2	−6.4
ERP/ERF attention	−23.0	−67.3	−3.9
	24.3	−65.3	−4.4

Talairach coordinates in the left and right hemispheres of significant group-averaged fMRI activations and modeled dipolar sources for the grand average ERP/ERF difference fields corresponding to the sensory and attention effects are shown.

Data analysis. Separate ERP and ERF averaged waveforms time-locked to motion onset were derived for each of the six trial types (three stimulus conditions × two attention conditions; see Table 1 and Fig. 1). Only responses to the more frequent nontarget (slow) stimuli were analyzed here. To determine the sensory effect of the presence of color, difference waves were formed by subtracting the ERP/ERF waveforms elicited on the no color-change trials from those on trials when the dots moving in the unattended direction changed to red. To determine the effect of attention on color processing, difference waves were formed by subtracting the ERP/ERF waveforms on trials where the dots moving in the unattended direction changed to red from those where the attended-direction dots changed to red. Effects were quantified as mean amplitude measures over specified latency intervals (with respect to a 200-ms prestimulus baseline) at the sensor/electrode sites showing the largest amplitudes and tested with repeated-measures analysis of variance (ANOVA). To determine the time of onset of the sensory and attention effects, mean amplitude measures were taken over successive 10-ms intervals and tested by ANOVA for deviation from baseline ($P < 0.05$ criterion); the first of five successive 10-ms intervals meeting this criterion was considered the onset time.

Source analysis was carried out by using multimodal neuroimaging software CURRY 4.0 (Neuroscan). ERP and ERF surface field distributions were fitted in conjunction to obtain maximal localization power (21). Source modeling was performed by using regional equivalent current dipoles in a realistic boundary element model of the head derived from a structural magnetic resonance scan. Dipoles were modeled to fit to the grand average ERP/ERF difference fields by using the boundary element model from the subject whose brain dimensions were closest to the mean of all subjects (22). The following procedure was used for source modeling. The difference field was first modeled by using a single, unconstrained, equivalent current dipole. Because these single-dipole models explained <90% of the field variance, however, a second dipole had to be added. During the iterative best-fitting estimation calculations, the dipoles were allowed to move within the volume conductor without any constraints. This iterative best-fitting procedure resulted in these two dipoles settling into symmetrical locations in inferior occipital cortex of the left and right hemispheres.

MRI. Subjects were scanned with a neurooptimized GE Signa LX 1.5-T system (General Electric). In a structural session, whole-head T1-weighted images (spatial resolution, 1.0 × 1.0 × 1.5 mm; in-plane matrix, 256 × 256; 124 slices, no gap) were acquired with

PSYCHOLOGY

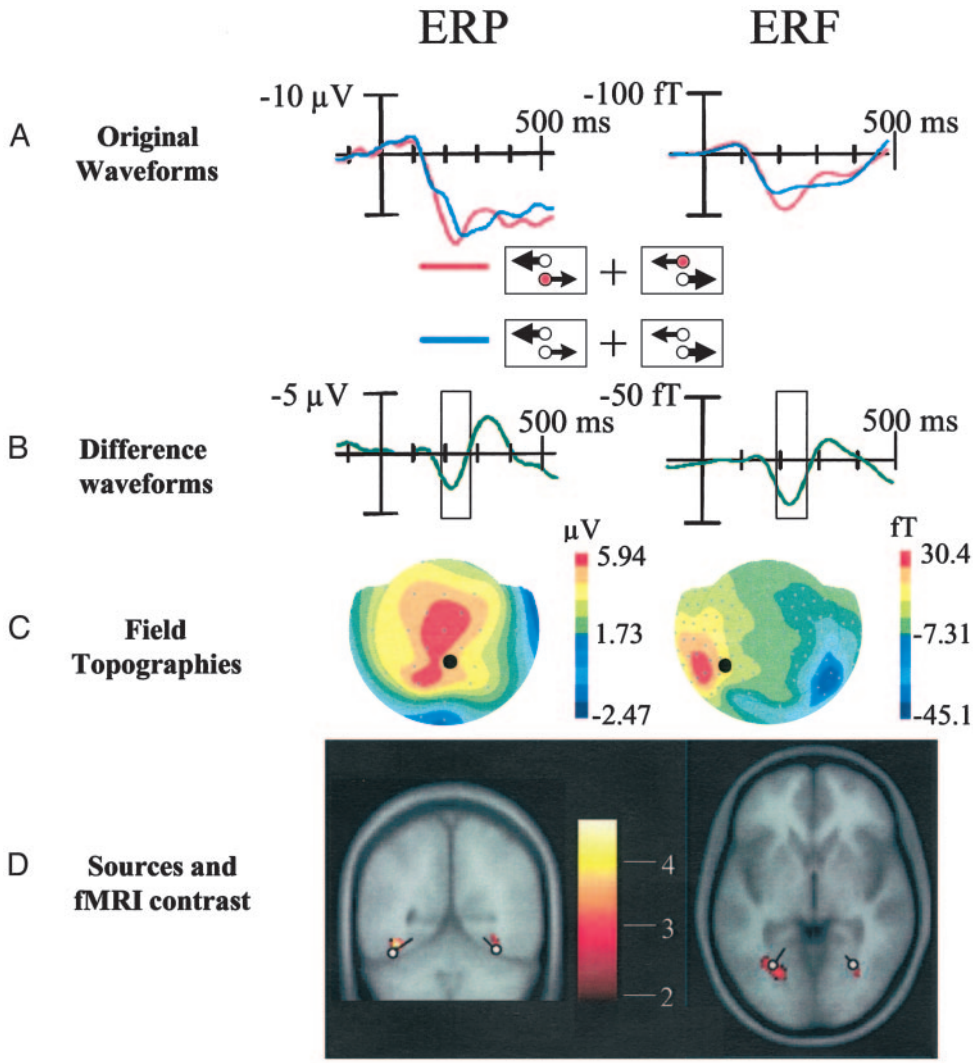

Fig. 2. The sensory effect of color. (*A*) Concurrently recorded ERP and ERF waveforms averaged over all subjects on trials with no color change accompanying dot movement (blue tracings) and on trials where dots moving in the unattended direction changed to red (red tracings). Waveforms are averaged over attend-left and attend-right conditions. Time 0 of recording epoch is when dot arrays begin to move. (*B*) Difference waveforms formed by subtracting the color-absent from the color-present waveforms shown in *A*. (*C*) Topographical field distributions of difference ERPs and ERFs shown in *B* for the time range of 180–250 ms. Black dots are recording sites for waveforms shown in *A* and *B*. (*D*) Locations of estimated source dipoles accounting for the surface topography of the difference ERP and ERF waveforms shown in *C*, together with fMRI activations in the corresponding sensory color contrast (trials with color change in dots moving in unattended direction versus trials with no color change). Dipoles and fMRI activations are superimposed on axial and coronal sections of the standard Montreal Neurological Institute brain.

a quadrature head coil by using a three-dimensional spoiled gradient echo sequence (repetition time/echo time/flip angle = 24 ms/8 ms/24°).

For the functional session, a 5-inch surface coil was centered beneath the subjects' occipital pole. During task performance, functional data from 20 slices (matrix, 64 × 64; field of view, 18 cm; slice thickness, 3 mm; no gap, orientation perpendicular to the calcarine fissure) covering the occipital cortex were collected by using an echo-planar imaging gradient echo sequence (repetition time/echo time/flip angle = 2,000 ms/40 ms/80°, ramp sampling on). The experiment consisted of six runs, each lasting 8–9 min (260 volumes).

fMRI: Eye-movement control. During functional runs, a video recording showing movements of the left eye of the subject was obtained by means of an infrared-light transmission device and fiber-optic cable. The resolution of this system for the detection of eye movements was better than 0.5°. Performance was monitored online, and all subjects were able to maintain fixation with <1° deviation.

fMRI analysis. Data from each subject were analyzed at first individually (SPM99, Wellcome Department of Cognitive Neurology, University College, London). The first four images of each run were removed to exclude saturation effects. The images were time-sliced, realigned to the fifth scan of the first run, normalized on the Montreal Neurological Institute template, resliced to 2 × 2 × 2 mm^3 cubic voxels, and spatially smoothed (Gaussian kernel, 6 mm). Individual anatomical scans were coregistered with the functional images and normalized to 2 × 2 × 2 mm^3 to serve as an overlay for the activated areas.

Functional data were temporally high- and low-pass-filtered and rescaled to the global mean. Statistical analysis of the data was performed by using the standard hemodynamic-response function in an event-related design for each subject (SPM99). Group analyses were performed by using the fixed effects model

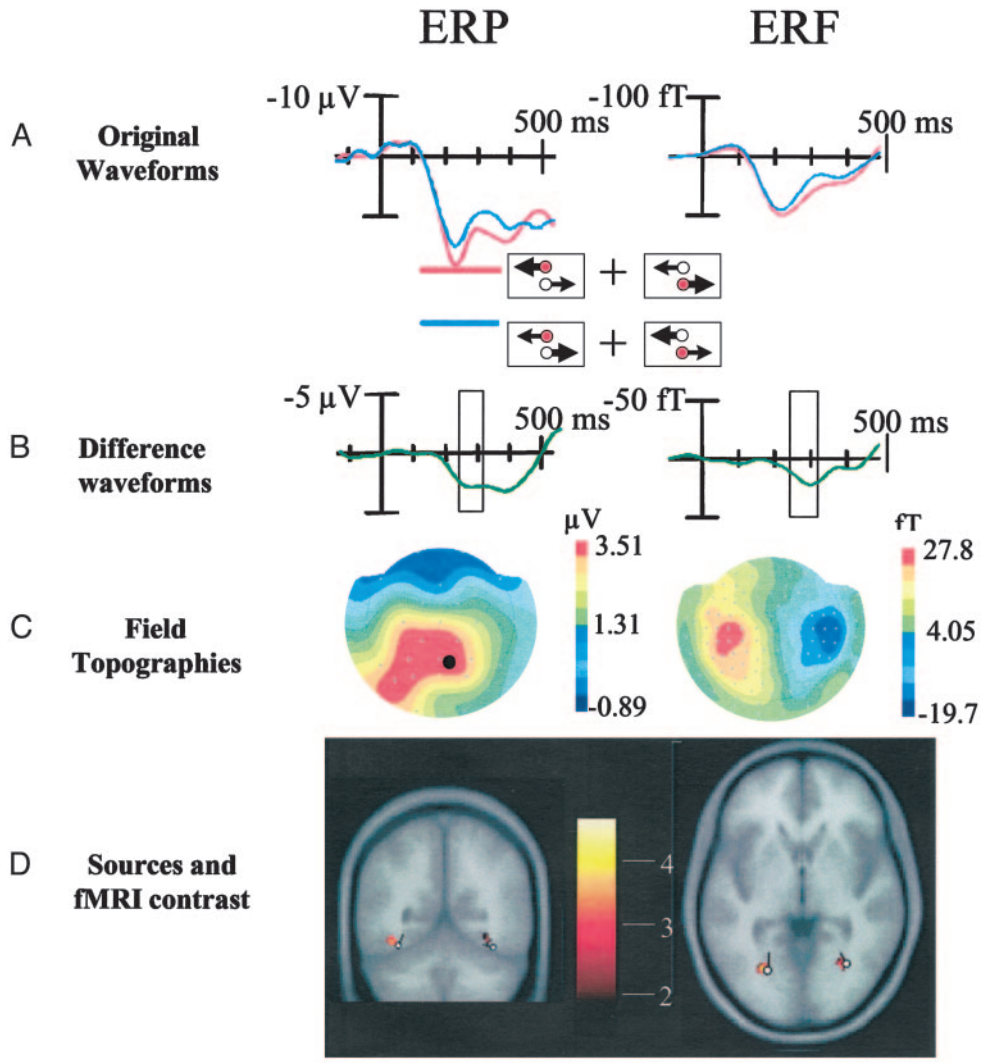

Fig. 3. The effect of attention on irrelevant color processing. (*A*) Concurrently recorded ERP and ERF waveforms averaged over all subjects on trials where the dots moving in the attended (red tracings) or unattended (blue tracings) direction changed color to red. Waveforms are averaged over attend-left and attend-right conditions. (*B*) Difference waveforms formed by subtracting the blue from the red waveforms shown in *A*. (*C*) Topographical field distributions of the difference waveforms shown in *B* for the time range of 220–300 ms. Black dots are the recording sites for waveforms shown in *A*. (*D*) Locations of estimated source dipoles accounting for the topography of the difference waveforms shown in *C* and corresponding fMRI activations for the attention effect on irrelevant color processing (contrast between trials where attended versus unattended dot arrays changed color).

approach. The effects were thresholded at $P = 0.01$, corrected for multiple comparisons and for cluster size (23). For coregistration, fMRI and ERP/MEF data were brought into the Montreal Neurological Institute space frame. The coordinates of the electromagnetic sources and fMRI activations were then transformed into Talairach space coordinates by using the mni2tal-transform (www.mrc-cbu.cam.ac.uk/Imaging/mnispace.html).

Results

Behavioral Responses. Subjects were accurate at detecting the faster moving-target dot arrays, with mean hit rates ranging from 88% to 93% and false-alarm rates from 1.6% to 2.1% under the different conditions. Mean reaction times (RTs) ranged from 654 to 703 ms. There were no significant differences in detectability or RT between the left- and right-moving targets: hit rate, $F(1, 7) = 0.01$, not significant (ns); false-alarm rate, $F(1, 7) = 0.31$, ns; and RT, $F(1, 7) = 0.83$, ns. More importantly, the color configuration of the moving-dot arrays (comparing attended-red/unattended-white, attended-white/unattended-red, and attended-white/unattended-white) did not affect detection performance: hit rate, $F(2, 14) = 0.11$, ns; false-alarm rate, $F(2, 14) = 0.10$, ns; and RT, $F(2, 14) = 0.52$, ns. These factors of target direction and color configuration did not interact significantly.

Sensory Effect of Color. The ERP to the onset of dot movement included a broadly distributed positive wave that onset at ≈100 ms and peaked at 200–250 ms (Fig. 2*A*). When an irrelevant color change was added to the dot array moving in the unattended direction, an additional positivity was elicited in the 150- to 250-ms interval relative to when no color was present. This "sensory effect" of color (collapsed over attend-left and attend-right conditions and measured over 190–240 ms) was significant in both the ERP [$F(1, 7) = 7.26$, $P < 0.03$] and ERF [$F(1, 7) = 19.45$, $P < 0.003$] recordings. The time course of the sensory color effect can be seen in the difference waveforms formed by subtracting the ERP/ERF waveforms elicited in the no-color conditions from those elicited when the color of the unattended surface changed to red (Fig. 2*B*). The surface topography of these difference waveforms had a midline central-parietal max-

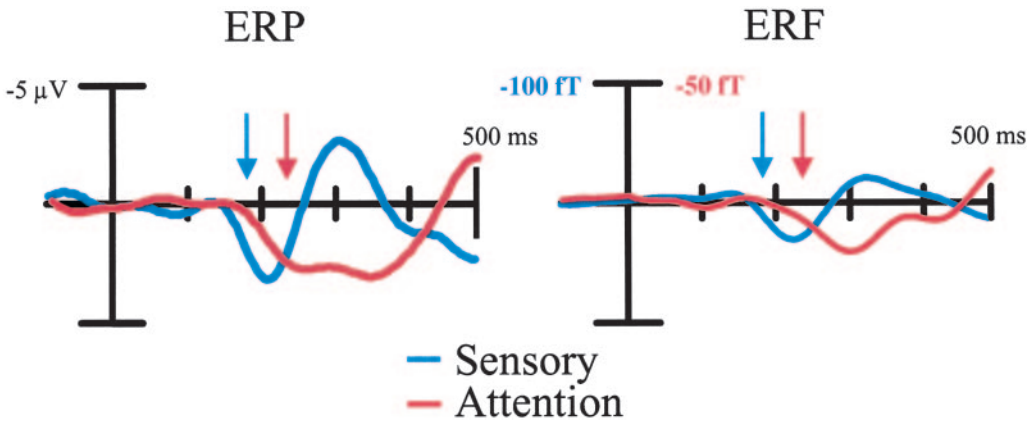

Fig. 4. Timing of sensory color and attention effects. Difference waveforms for the sensory color effect (blue tracings, from Fig. 2*B*) are superimposed with the difference waveforms for the attention effect (red tracings, from Fig. 3*B*). The arrows indicate earliest times (tested in successive 10-ms intervals) at which these difference waveforms deviated significantly from the prestimulus baseline.

imum in the ERP and occipitotemporal maxima and minima in the ERF (Fig. 2*C*). Source analysis indicated that a pair of dipolar neural generators in the ventral occipital cortex (left and right fusiform gyri) accounted for 94% of the variance in the surface-recorded ERP/ERF difference fields (Fig. 2*D*). The dipoles in the left and right hemispheres were approximately symmetrical in position, and they produced lateralized ERF foci of opposite polarity following the right-hand rule of magnetic field generation.

In the separate sessions with event-related fMRI, the corresponding sensory color contrast (color change in unattended dots versus no color change) revealed two symmetrical foci of activation (both $P < 0.01$, corrected) in the left and right fusiform gyri. These sites of enhanced hemodynamic response to the colored stimuli were spatially coincident with the dipolar sources calculated from the corresponding ERP/ERF difference waveforms (Fig. 2*D* and Table 1).

Attention Effect on Irrelevant Color Processing. The effect of attention on the neural activity elicited by the irrelevant color feature was assessed by comparing the ERP/ERF waveforms on trials where the dot array moving in the attended direction changed color versus trials having the same stimuli but with the unattended dots changing color (Fig. 3*A*). This "attention effect" comparison (collapsed over attend-left and attend-right trials) showed enhanced ERP/ERF amplitudes over the 200- to 400-ms range when the attended dots changed color. This attention effect (measured over 230–280 ms) was significant for both the ERP [$F(1, 7) = 8.59$, $P < 0.02$] and ERF [$F(1, 7) = 21.45$, $P < 0.002$] recordings (Fig. 3*B*). The surface topography of the attention effect (Fig. 3*C*) could be accounted for by a pair of dipolar sources in the fusiform gyrus, which accounted for 92% of the variance in the ERP/ERF difference fields (Fig. 3*D*).

In the fMRI sessions, the attention-effect contrast between trials with the attended versus the unattended dot arrays changing color revealed two foci of activity (both $P < 0.01$, corrected) located in the left and right fusiform gyri (Fig. 3*D*). These foci of increased activity on trials where the attended dots changed color were spatially coincident with the dipolar sources calculated from the corresponding ERP/ERF difference waveforms (Fig. 3*D* and Table 1).

Comparison of Timing of Sensory and Attention Effects. The fMRI results showed that the increased neural activity corresponding to the sensory color effect was localized to the same region of the fusiform gyrus as the enhanced activity corresponding to the attention effect (Table 1). The locations of the calculated dipolar sources of the ERP/ERF difference waveforms for the sensory and attention effects were virtually identical to these sites of fMRI activation. The relative timing of these two effects can be seen by comparing their respective difference waveforms (Fig. 4). The sensory color effect became significantly different from baseline at 180–190 ms in the ERP and 190–200 ms in the ERF, whereas the attention effect became significant at 240–250 ms in the ERF and 230–240 ms in the ERP.

Discussion

The present study used hemodynamic (fMRI) and electromagnetic (ERP/ERF) measures to define the timing as well as the localization of brain activity linked with the processing of an irrelevant color feature of an attended moving-dot array. Such arrays are perceived as coherently moving transparent surfaces, which may be attended selectively as unitary objects (refs. 8 and 24; see also ref. 25). The behavioral results (target detection accuracy and RT) confirmed that stimulus color was in fact irrelevant to task performance. The converging fMRI and ERP/ERF data indicated that processing of the irrelevant color feature in ventral occipital cortex was enhanced when it belonged to the attended surface, thus reinforcing previous physiological evidence that multifeature objects can serve as the units of visual attention (20). Moreover the time course of the ERP and ERF waveforms showed that this irrelevant feature processing was facilitated quite rapidly, within ≈40–60 ms after the initial registration of the color information in the same cortical area. These findings provide strong support for the integrated-competition model of object-selective attention (18) and demonstrate that enhanced processing of the irrelevant feature occurs quickly enough to participate in the feature-binding processes that underlie the perceptual unity of attended objects.

The timing of feature selection and binding processes has been estimated on the basis of both physiological (ERP) and behavioral (RT) evidence. Previous studies have found that task-relevant visual features including color, orientation, shape, spatial frequency, and movement direction are selected in the time range of 120–180 ms after stimulus onset depending on cue discriminability (26, 27). The selection and binding of task-relevant conjunctions of these features usually entail an additional delay and become evident in the interval of 150–260 ms (28–30). The present ERP/ERF waveforms show that processing of the irrelevant feature of the attended object is enhanced in this same time frame (at 230–250 ms) and therefore could provide a neural basis for the perceptual integration of the multiple features of the object. Given the low temporal resolution of fMRI, use of this method alone would not have been able

to distinguish such an early facilitation from a delayed associative activation that followed perceptual processing.

Enhanced neural activity associated with the presence of color in the unattended surface (sensory effect) was localized by using fMRI to the same region of the fusiform gyrus, as was the more pronounced increase in activity elicited when the attended surface was colored (attention effect). Dipole modeling of the ERP/ERF components associated with the sensory-color and attention effects (starting at ≈190 and 230 ms after stimulus onset, respectively) showed that both effects could be attributed to neural generators in this same fusiform region. This spatial coincidence strongly suggests that the hemodynamic and electromagnetic measures, obtained under identical experimental conditions, were detecting the same neural activity patterns. Previous studies have shown that this ventral-occipital fusiform area (with Talairach coordinates in the range of $x = 19–33$, $y = -63$ to -74, and $z = 0$ to -12) is involved in representing color information (31–33) and shows enhanced activity during attention to color (2, 34, 35). The present results thus are in accord with the integrated-competition model (18, 19), which posits that the neural basis for the perceptual integration of an attended object includes enhanced activity in the network of specialized modules that encode its individual features, including those that are not relevant to the immediate task.

According to Treisman's feature-integration theory (14), the various features belonging to an object become bound together as a consequence of spatial attention being directed to the location of the object. Although this theory has wide applicability, it does not seem possible that spatially focused attention could effectively distinguish one surface from another in the case of dense, overlapped moving-dot arrays such as those used here (8, 24). The integrated-competition model (18, 19) offers an alternative framework for addressing the binding problem that fits well with the present results. In this view, directing attention to one of an object's features produces a competitive advantage for the object in the neural module encoding that feature, which then is transmitted to the modules encoding the other features of the object. The resulting activation of the entire network of specialized modules would then underlie the binding of features into a unified perceptual object. Although questions remain about how this linkage between modules might be achieved (19, 20, 36), the present findings point to a dynamic neural substrate for the rapid perceptual integration of multifeature objects and provide critical data on the timing of feature selection and binding processes that can be incorporated into both neural and psychological models of object-selective attention.

This work was supported by Deutsche Forschungsgemeinschaft Grant HE-1531/3-5, Bundesministerium für Bildung und Forschung Grant 01GO00202, and National Institute of Mental Health Grant MH-25594-29.

1. Posner, M. I., Snyder, C. R. & Davidson, B. J. (1980) *J. Exp. Psychol.* **109,** 160–174.
2. Corbetta, M., Miezin, F. M., Dobmeyer, S., Shulman, G. L. & Petersen, S. E. (1991) *J. Neurosci.* **11,** 2383–2402.
3. Wolfe, J. M., Friedman-Hill, S. R. & Bilsky, A. B. (1994) *Percept. Psychophys.* **55,** 537–550.
4. Rossi, A. F. & Paradiso, M. A. (1995) *Vision Res.* **35,** 621–634.
5. Driver, J. & Baylis, G. (1998) in *The Attentive Brain*, ed. Parasuraman, R. (MIT Press, Cambridge, MA), pp. 299–325.
6. Lamy, D. & Egeth, H. (2002) *Percept. Psychophys.* **64,** 52–66.
7. Duncan, J. (1984) *J. Exp. Psychol. Gen.* **113,** 501–517.
8. Rodriguez, V., Valdes-Sosa, M. & Freiwald, W. (2002) *Brain Res. Cogn. Brain Res.* **13,** 187–193.
9. Blaser, E., Pylyshyn, Z. W. & Holcombe, A. O. (2000) *Nature* **408,** 196–199.
10. Kramer, A. F., Weber, T. A. & Watson, S. E. (1997) *J. Exp. Psychol. Gen.* **126,** 3–13.
11. Law, M. B. & Abrams, R. A. (2002) *Percept. Psychophys.* **64,** 1017–1027.
12. Egly, R., Driver, J. & Rafal, R. D. (1994) *J. Exp. Psychol. Gen.* **123,** 161–177.
13. Abrams, R. A. & Law, M. B. (2000) *Percept. Psychophys.* **62,** 818–833.
14. Treisman, A. (1998) *Philos. Trans. R. Soc. London B* **353,** 1295–1306.
15. Desimone, R. & Duncan, J. (1995) *Annu. Rev. Neurosci.* **18,** 193–222.
16. Reynolds, J. H., Chelazzi, L. & Desimone, R. (1999) *J. Neurosci.* **19,** 1736–1753.
17. Recanzone, G. H. & Wurtz, R. H. (2000) *J. Neurophysiol.* **83,** 777–790.
18. Duncan, J. (1996) in *Attention and Performance XVI*, ed. McClelland, J. L. (MIT Press, Cambridge, MA), pp. 549–578.
19. Duncan, J., Humphreys, G. & Ward, R. (1997) *Curr. Opin. Neurobiol.* **7,** 255–261.
20. O'Craven, K. M., Downing, P. E. & Kanwisher, N. (1999) *Nature* **401,** 584–587.
21. Fuchs, M., Wagner, M., Wischmann, H. A., Kohler, T., Theissen, A., Drenckhahn, R. & Buchner, H. (1998) *Electroencephalogr. Clin. Neurophysiol.* **107,** 93–111.
22. Schoenfeld, M. A., Woldorff, M. G., Düzel, E., Scheich, H., Heinze, H.-J. & Mangun, G. R. (2003) *J. Cogn. Neurosci.* **15,** 157–172.
23. Poline, J. B., Worsley, K. J., Evans, A. C. & Friston, K. J. (1997) *Neuroimage* **5,** 83–96.
24. Reynolds, J. H., Alborzian, S. & Stoner, G. R. (2003) *Vision Res.* **43,** 59–66.
25. He, Z. J. & Nakayama, K. (1995) *Proc. Natl. Acad. Sci. USA* **92,** 11155–11159.
26. Anllo-Vento, L. & Hillyard, S. A. (1996) *Percept. Psychophys.* **58,** 191–206.
27. Kenemans, J. L., Lijffijt, M. Camfferman, G. & Verbaten, M. N. (2002) *J. Cognit. Neurosci.* **14,** 48–61.
28. Karayanisis, F. & Michie, P. T. (1997) *Electroencephalogr. Clin. Neurophysiol.* **103,** 282–297.
29. Cortese, F., Bernstein, L. J. & Alain, C. (1999) *NeuroReport* **10,** 1565–1570.
30. Smid, H. G. O. M., Jakob, A. & Heinze, H.-J. (1999) *Psychophysiology* **36,** 264–279.
31. McKeefry, D. J. & Zeki, S. (1997) *Brain* **120,** 2229–2242.
32. Hadjikhani, N., Liu, A. K., Dale, A. M., Cavanagh, P. & Tootell, R. B. (1998) *Nat. Neurosci.* **1,** 235–241.
33. Sakai, K., Watanabe, E., Onodera, Y., Uchida, I., Kato, H., Yamamoto, E., Koizumi, H. & Miyashita, Y. (1995) *Proc. R. Soc. London Ser. B* **261,** 89–98.
34. Clark, V. P., Parasuraman R., Keil, K., Kulansky, R., Fannon S., Maisog, J. M., Ungerleider, L. G. & Haxby J. V. (1997) *Hum. Brain Mapp.* **5,** 293–297.
35. Anllo-Vento, L., Luck, S. J. & Hillyard, S. A. (1998) *Hum. Brain Mapp.* **6,** 216–238.
36. Singer, W. (2001) *Ann. N.Y. Acad. Sci.* **929,** 123–146.